Macromolecules

pubs.acs.org/Macromolecules

Article

Linear Catenanes in Channel Confinement

Pietro Chiarantoni and Cristian Micheletti*

Cite This: *Macromolecules* 2023, 56, 2736−2746

Read Online

ACCESS | Metrics & More | Article Recommendations | Supporting Information

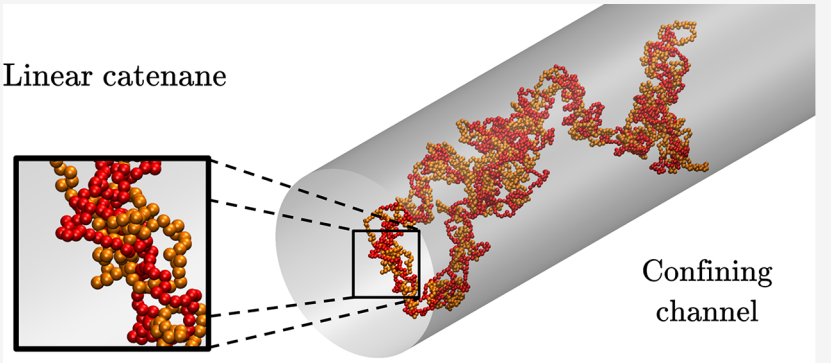

ABSTRACT: We use Langevin dynamics simulations to investigate the behavior of linear catenanes under channel confinement. We consider model poly[*n*]catenanes of $n = 100$ rings, each of $m = 40$ beads, and present a comprehensive analysis of their statics and dynamics in cylindrical channels of various diameters. To highlight the impact of mechanical bonding, we compare the catenane behavior to an equivalent chain of beads under the same conditions. We show that linear catenanes exhibit various confinement regimes, including a de Gennes one for intermediate channel widths and an overstretching response for strong confinement, which is unique to catenanes. The catenane's relaxation dynamics also diverge from conventional polymers at strong confinement, presenting much slower modes. Through systematic analysis of the size, shape, and orientation of the concatenated rings and their mechanical bonds, we shed light on the underlying mechanisms driving the catenane's static and dynamic responses to confinement.

INTRODUCTION

Recent breakthroughs in the synthesis of linear catenanes,[1,2] supramolecular structures made of a linear succession of mechanically bonded rings, have boosted interest for their applicative potential, ranging from molecular recognition and catalysis to materials science,[3−11] as well as for understanding their unique properties, especially those afforded by mechanical bonding.[12−21]

In this respect, much insight was obtained by contrasting the metric and dynamic properties of catenanes in bulk with those of conventional, i.e., covalently bonded, linear polymers. The comparisons helped establish how the size and number of constitutive rings differently contribute to the scaling of the gyration radius,[16,22] often introducing significant corrections to the asymptotic scaling expected for equivalent self-avoiding chains. In addition, different models have shown that, at small scales, the Rouse-like relaxation modes seen in linear polymers are replaced by slower ones in mechanically bonded chains of rings.[11,15,23,24]

These ongoing efforts have significantly advanced our understanding of isolated and interacting catenanes in bulk.[15,16,22−27] However, except for Hopf links,[28,29] no characterization exists yet of catenanes in spatial confinement, despite it being a natural avenue considering the body of knowledge available for conventional polymers in channels and slits. These systems present different metric scaling regimes depending on how the confining region width compares with the polymer length scales, such as thickness, contour length, and persistence length.[30−40] Examining catenanes in confinement thus provides a unique opportunity to study the impact of additional degrees of freedom, such as changes in ring size and mechanical bonds, on the overall metric and dynamic properties.

Here we present a first systematic study tackling these questions. We consider a model polycatenane made of 100 fully flexible rings of 40 beads and examine the statics and dynamics in cylindrical channels of various widths. We additionally consider equivalent chains of beads, and the comparison allows us to isolate properties with no analogue in linear polymers.

Received: February 12, 2023
Revised: March 11, 2023
Published: March 27, 2023

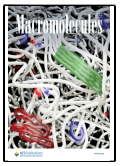

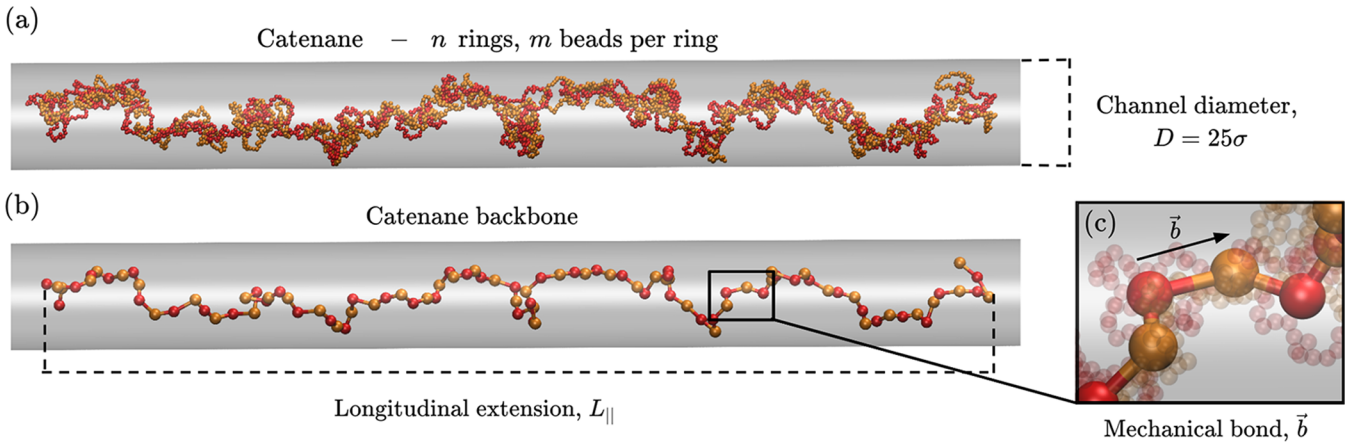

Figure 1. Polycatenanes in channel confinement: model and definitions. (a) Typical configuration of a poly[n]catenane of n = 100 rings, each of m = 40 beads, confined in a channel with diameter $D = 25\sigma$. Alternating ring colors are used for clarity. Panel b shows the corresponding backbone of the catenane, joining the rings' centers of mass (beads). The backbone's footprint projected on the channel axis is used to define the longitudinal extension of the catenane, $L_{\|}$. A magnified view of the backbone, with the constitutive rings in overlay, is shown in (c), where a specific mechanical bond is highlighted.

Our findings show that linear catenanes exhibit a range of confinement regimes, including a de Gennes one for intermediate channel widths and an overstretching response for strong confinement, unique to catenanes. Due to slower relaxation modes, internal dynamics also differs from that of linear polymers, especially under strong confinement. The underlying mechanisms driving these effects are examined with a multiscale analysis of various observables, such as the size, shape, and orientation correlation of the rings and mechanical bonds.

MODEL AND METHODS

Model Definition and Simulation Setup. As a model poly[n]catenane, we considered a succession of n = 100 mechanically bonded rings, each consisting of m = 40 beads (monomers). Pairs of consecutive rings are interlocked in a Hopf-link topology; see Figure 1.

The rings are fully flexible, and the excluded volume interaction of any pair of monomers (both intra- and inter-ring) is described with a truncated and shifted Lennard-Jones (Weeks–Chandler–Anderson, WCA) potential:

$$U_{\mathrm{LJ}} = \begin{cases} 4\epsilon\left[\left(\frac{\sigma}{r}\right)^{12} - \left(\frac{\sigma}{r}\right)^{6} + \frac{1}{4}\right] & r \le 2^{1/6}\sigma \\ 0 & \text{otherwise} \end{cases} \quad (1)$$

where σ is the nominal diameter of the beads and the potential amplitude is taken equal to the canonical thermal energy of the system, $\epsilon = k_{\mathrm{B}}T$. The characteristic length and energy scales, σ and ϵ, are taken as the length and energy units, respectively, and the bead mass M is taken as the mass unit. These choices also define the Lennard-Jones time scale $\tau_{\mathrm{LJ}} = \sigma\sqrt{M/\epsilon}$.

The chain connectivity of the rings is provided by a standard finite extensible nonlinear elastic (FENE) interaction of consecutive beads, resulting from the sum of the above LJ repulsion and an attractive FENE term:[41]

$$U_{\mathrm{FENE}} = \begin{cases} -0.5k_{\mathrm{FENE}}R_0^{\,2}\ln\left(1 - \left(\frac{r}{R_0}\right)^2\right) & r \le R_0 \\ \infty & r > R_0 \end{cases} \quad (2)$$

with $k_{\mathrm{FENE}} = 30\epsilon/\sigma^2$ and $R_0 = 1.5\sigma$.

The catenane was confined in a cylindrical channel, whose nominal radius was varied from 3σ to 70σ. Excluded volume interactions with the channel walls were treated with the same repulsive potential of eq 1, with r now being the bead–wall distance. The effective channel diameter, D, associated with each nominal radius was established *a posteriori*. To do so, we projected all sampled configurations on the transverse plane, i.e., the plane orthogonal to the channel axis. The effective diameter was then computed as the maximum distance in the transverse plane of any two monomers plus σ, the nominal diameter of the monomers; see Figure S1.

The Langevin dynamics simulations of the catenanes in confinement were conducted using the LAMMPS software package,[42] using a standard friction coefficient[41] and a periodic parallelepiped simulation box, which was long enough to prevent the confined catenane to interact with its periodic images. The simulations were integrated with a time step of $5 \times 10^{-3}\tau_{\mathrm{LJ}}$, where τ_{LJ} is the characteristic Lennard-Jones time. We collected five independent trajectories for each channel width, each of duration $5 \times 10^{6}\tau_{\mathrm{LJ}}$ or more, largely exceeding the slowest relaxation modes of the system; see Results. Observables were averaged over all trajectories, and their statistical uncertainties were estimated from the dispersion (error of the mean) of the averages taken separately for each trajectory.

Observables. *Catenane Backbone.* Several observables for the statics and dynamics were defined in terms of the catenane's mechanical backbone, which is determined by the succession of the centers of mass of the rings; see Figure 1. The mechanical bonds, embodied by the vectors connecting the centers of mass (CoMs) of two consecutive (linked) rings, do not have a fixed length due to the variable interpenetration of the rings (Figure 1c). The effective persistence length of the backbone $l_{\mathrm{p}}^{\mathrm{bulk}}$ was obtained from the decay of the orientational

https://doi.org/10.1021/acs.macromol.3c00249
Macromolecules 2023, 56, 2736–2746

Table 1. Global Metric Properties of the Model Catenane in Channel Confinement and Comparison with Equivalent Chain[a]

	catenane backbone			equivalent chain		
D/σ	$L_\parallel/\sigma$	R_g/σ	$R_\parallel/\sigma$	$L_\parallel/\sigma$	R_g/σ	$R_\parallel/\sigma$
8	604.9 ± 0.4	155.0 ± 0.1	155.0 ± 0.1	465.2 ± 0.1	135.6 ± 0.1	135.6 ± 0.1
15	352.4 ± 0.5	103.3 ± 0.2	103.1 ± 0.2	353.0 ± 0.1	103.6 ± 0.1	103.5 ± 0.1
50	144.9 ± 4.0	46.0 ± 0.9	44.3 ± 1.0	130.2 ± 1.0	43.0 ± 0.9	41.3 ± 1.1
∞	77.8 ± 3.2	38.6 ± 1.2	22.0 ± 1.3	79.0 ± 1.2	39.7 ± 0.6	24.0 ± 0.5

[a]The average values of the catenane's longitudinal extension ($L_\parallel$), gyration radius (R_g), and its longitudinal component ($R_\parallel$) are provided for three different diameters of the confining channel, D/σ = 8, 15, and 50, and for the unconstrained case, too, indicated with $D = \infty$. Analogous quantities are provided for the equivalent chain.

correlation function of the normalized mechanical bonds of catenanes in bulk (unconstrained).

Static Properties. We considered the average longitudinal span $L_\parallel$ of the catenane's backbone, corresponding to the maximum distance of any two rings' CoMs projected along the channel axis; see Figure 1b. Inspired by studies of backfolds in channel-confined polymers,[43] we additionally analyzed the fraction of mechanical bonds that are backfolded with respect to the catenane's end-to-end vector. We considered as backfolded those bonds for which $\hat{b}\cdot\hat{R}_{ee} \leq \cos(\theta)$, with $\theta = \{\pi/2, 2\pi/3\}$. In the above expression, $\hat{b}$ and $\hat{R}_{ee}$ are the normalized bond and end-to-end vectors.

We studied the geometry of the catenated rings by computing their instantaneous gyration tensors:

$$Q_{\alpha\beta} = \frac{1}{m}\sum_{i=1}^{m} r_i^{(\alpha)} r_i^{(\beta)} - \frac{1}{m^2}\sum_{j=1}^{m} r_j^{(\alpha)} \sum_{k=1}^{m} r_k^{(\beta)} \tag{3}$$

where $r_i^{(\alpha)}$ is the αth Cartesian coordinate of the ith bead in the ring, obtaining the principal eigenvalues, ${\lambda_1}^2 \geq {\lambda_2}^2 \geq {\lambda_3}^2$ and corresponding (normalized) eigenvectors, $\hat{e}_1$, $\hat{e}_2$, and $\hat{e}_3$. We characterized the typical size and shape of single rings in the catenane through the λ's of the central one, subsequently averaging the observables over trajectories. The third principal axis, $\hat{e}_3$, was used to determine the spatial orientation of a ring, as it is orthogonal to the ring's osculating plane. The orientational correlation of two rings, i and j, was measured as $\langle|\hat{e}_3^i\cdot\hat{e}_3^j|\rangle$, where the brackets denote the average over trajectories and the absolute value to discount the "up/down" orientation of $\hat{e}_3$, as the direction is physically irrelevant.

Dynamic Properties. For the global relaxation dynamics we examined the autocorrelation function of the longitudinal extension:

$$C_\parallel(\tau) = \frac{\langle (L_\parallel(t+\tau) - \overline{L}_\parallel)\cdot(L_\parallel(t) - \overline{L}_\parallel)\rangle_t}{\langle (L_\parallel(t) - \overline{L}_\parallel)^2\rangle_t} \tag{4}$$

where $\langle\ \rangle_t$ represents averaging over time and $\overline{L}_\parallel$ is the ensemble average of the longitudinal extension computed over all trajectories. We obtained the characteristic relaxation time integration:

$$\tau_\parallel = \int_0^\infty C_\parallel(\tau)\, d\tau \tag{5}$$

The numerical integration was performed up to the point where $C_\parallel(\tau)$ dropped below 10^{-2}, and it was carried out separately for each independent trajectory, obtaining uncorrelated estimates for $\tau_\parallel$ at each considered channel width. The estimates were used to compute the mean $\tau_\parallel$ and its statistical uncertainty.

For the local relaxation dynamics we examined the autocorrelation function of the longitudinal projection of the central mechanical bond, $b_\parallel$.

We further examined the characteristic reorientation time of the rings,[44] τ_{TACF}. Following ref 45, we consider the generalization to circular chains of the time-lagged terminal autocorrelation function (TACF) of linear chains:

$$C_{TACF}(\tau) = \langle \hat{d}_{i,i+m/2}(t+\tau)\cdot\hat{d}_{i,i+m/2}(t)\rangle_{t,i} \tag{6}$$

where $\hat{d}_{i,i+m/2}$ is the normalized distance vector (diameter) of beads i and $i + m/2$; $\langle\ \rangle_{i,t}$ indicates averaging over time and bead index i. C_{TACF} thus measures the time-lagged orientational correlation of all diameters of the ring of interest. We computed τ_{TACF} by integrating C_{TACF} for the central ring in the chain, again treating each trajectory separately.

Equivalent Chain. We compared the properties of catenanes with those of equivalent covalently bonded chains of beads. Following ref 24, this comparison was established in the bulk (unconstrained) case using the following mapping: (i) each ring in the catenane was represented by a single bead in the equivalent chain, with a size $\tilde{\sigma}$ such that the bond length of the equivalent polymer matches the average mechanical bond length of the catenane backbone; (ii) the equivalent chain was given an effective bending rigidity that was adjusted to match the average gyration radius of the catenane; (iii) the mass of an equivalent bead was set equal to the total mass of one ring; (iv) the Langevin friction coefficient of an equivalent bead was set equal to m times that of the ring's monomers. With this proviso, the diffusion coefficients of the entire catenane and the equivalent chain are matched.

The equivalent chains were confined in cylindrical channels of various nominal widths. Analogously to the case of catenanes, the corresponding effective diameters, D, were established from the transverse projection of the sampled configurations, taking the maximum transverse distance of the equivalent monomers and adding to it $\tilde{\sigma}$. The parameters of the mapping are given in Table S1.

Note that the above mapping establishes the equivalence of the static and dynamics of the two systems exclusively in the unconstrained (bulk) case and purposely maintains the bulk-case parametrization at all levels of confinement. This approach allows for investigating the differences between the two systems by directly comparing their metric and dynamic properties for varying channel widths.

For its direct nature, we favored this approach over the alternative one of reparametrizing the static and dynamic mappings of the two systems at each channel width. In this complementary scheme, the differences can instead be established by analyzing how the parameters of the mapping

https://doi.org/10.1021/acs.macromol.3c00249
Macromolecules 2023, 56, 2736−2746

(e.g., bead size, bending rigidity, friction coefficient) vary with D.

For completeness, we point out that other strategies could be adopted to isolate the effects of mechanical bonding. A noteworthy one was adopted in ref 27 to study the response of catenanes to mechanical stretching, a problem involving uniaxial elongations too, albeit of a different kind from channel confinement. In this study, a ring is covalently bonded to its neighbors at two diametrically opposite monomers, i.e., with contour distance equal to half the ring's contour length. This approach preserves the linear succession of rings while suppressing their mechanical bonding.

RESULTS

We studied the effect of channel confinement on the statics and dynamics of catenanes composed of $n = 100$ self-avoiding flexible rings, each with 40 monomers. The channel diameter, D, was varied from $D = 120\sigma$ to $D = 5\sigma$, covering different confinement regimes, from weak to strong. The range of D was determined with reference to the typical gyration radii of the entire catenane in bulk ($R_g = 38.6\sigma$) and that of its rings ($R_g^{ring} = 3.6\sigma$); see Tables 1 and 2.

Table 2. Local Metric Properties of the Model Catenane in Channel Confinement[a]

D/σ	b/σ	$b_\parallel/\sigma$	R_g^{ring}/σ	$R_\parallel^{ring}/\sigma$
8	5.6	5.5	3.4	2.6
15	4.5	3.8	3.6	2.2
50	4.8	3.0	3.6	2.1
∞	4.8	3.0	3.6	2.1

[a]The average values of the mechanical bond (b) and the gyration radius of concatenated rings (R_g^{ring}), and their longitudinal components, are provided for three different diameters of the confining channel, $D/\sigma = 8$, 15, and 50, and for the unconstrained case, too, indicated with $D = \infty$. Statistical errors are of the order of 1%.

Figure 2 displays global metric observables, the catenanes' longitudinal extension $L_\parallel$, and the gyration radius as a function of the channel width. The data is presented in log−log plots to aid the metric scaling analysis, with relevant length scales marked on the x-axis. Linear versions of the plots are provided in Figure S2.

At the largest channel widths, the extension of the catenanes is close to the average span in the unconstrained (bulk) case, 77.8σ, marked by a dashed line. The same holds for the equivalent chain, a conventional linear polymer defined by a 1:1 mapping of the monomers and the catenated rings; see Model and Methods. The mapping is established in the unconstrained (bulk) case and maintained fixed at all confinements. This approach was specifically designed to highlight the different behaviors elicited by channel confinement in catenanes and conventional chains that are otherwise equivalent in the unconstrained case.

Decreasing the channel diameter, D, below the gyration diameter of free catenanes ($\sim 77.2\sigma$) establishes the weak confinement regime. More precisely, its onset is marked by the minimum gyration radius of the catenane. As for ordinary polymers, the nonmonotonicity of R_g arises from the opposite trends of the longitudinal and transverse components of the gyration radius, which here occurs for $D \sim 80\sigma$; see Figure 2b. In weak confinement, the growing longitudinal extension of the catenane remains comparable to that of the equivalent polymer, which is systematically smaller by approximately 10%. Despite their completely different microscopic structures, the backbones of the catenane and the equivalent chain are similarly convoluted in space; see Figure 2c.

For conventional flexible polymers, as our equivalent chain, weak confinement is followed by the de Gennes scaling regime, where $L_\parallel \propto D^{(\nu-1)/\nu} \sim D^{-2/3}$. For asymptotically long chains, this regime manifests for $2l_p \lesssim D \lesssim R_g$.[32] For our system size, this corresponds to $18 \lesssim D/\sigma \lesssim 40$, given that the effective persistence length of unconstrained catenanes is close to 9σ, i.e., two mechanical bonds. In this range of D, the trend of the catenane's $L_\parallel$ is indeed close to the $D^{-2/3}$ scaling and, interestingly, more compatible with it than the equivalent chain. Figure 3 shows a substantial drop in the fraction of mechanical bonds directed backward with respect to the catenane's end-to-end vector, indicating that catenane's backfolds are disfavored, and more so than in equivalent chains; see also Figure S3.

Narrower channels, with diameters in the $l_p \lesssim D \lesssim 2l_p$ range, yield the so-called transition regime of conventional polymers.[32] Throughout this interval, which for our system corresponds to $9 \lesssim D/\sigma \lesssim 18$, the extensions of the catenane and equivalent polymer are nearly identical, with relative differences of about 2%. In this regime, backfolds are mostly absent, as seen in the typical conformations of Figures 2c and 3.

As D is taken below 9σ, both the catenane and equivalent polymer enter a strong confinement regime, where the channel diameter is close to the size of the unconstrained catenane's rings and the polymer's monomers, respectively. At this strong confinement, backfolds are suppressed (Figures 2c and 3) and the $L_\parallel$ curves of the two systems diverge. For the polymer, the extension plateaus close to the chain contour length, $L_\parallel \sim 480\sigma$. Instead, the catenane's extension varies with an even stronger dependence on D than in the de Gennes regime, the effective scaling exponent being about -1. The catenane's extension becomes significantly larger than the nominal contour length of the free catenane's backbone, $Nb^{bulk} \sim 480\sigma$, signaling dramatic deformations even at small scales. By analogy with mechanically induced structural deformations of double-stranded DNA,[46] we refer to this as the *overstretching* regime.

Mechanical Bond Stretching and Rings' Intermingling. The observed behavior of $L_\parallel$ poses the question of whether the overstretching regime is mainly caused by the extension of the rings or their increased separation. To clarify this point, we investigated the D dependence of two observables: the average gyration of single concatenated rings, R_g^{ring}, and the average length of mechanical bonds, b.

The results, shown in Figure 4, are noteworthy in several respects. First, both b and R_g^{ring} vary nonmonotonically with D, an effect due to the opposite trends of the longitudinal and transverse components. Second, the b and R_g^{ring} minima occur for very different channel widths. Specifically, b is minimum for $D \sim 13\sigma$, which is about twice the free catenane's persistence length, $2l_p^{bulk} \sim 18\sigma$. Notice that this channel width is well below the one minimizing the catenane's R_g, $D \sim 80\sigma$; see Figure 2b. Differently, the minimum of R_g^{ring} occurs for $D \sim 7\sigma$, which is about twice the gyration radius of single rings in unconstrained catenanes; see Table 2. Accordingly, this width marks the onset of the nominal weak confinement regime for

https://doi.org/10.1021/acs.macromol.3c00249
Macromolecules 2023, 56, 2736−2746

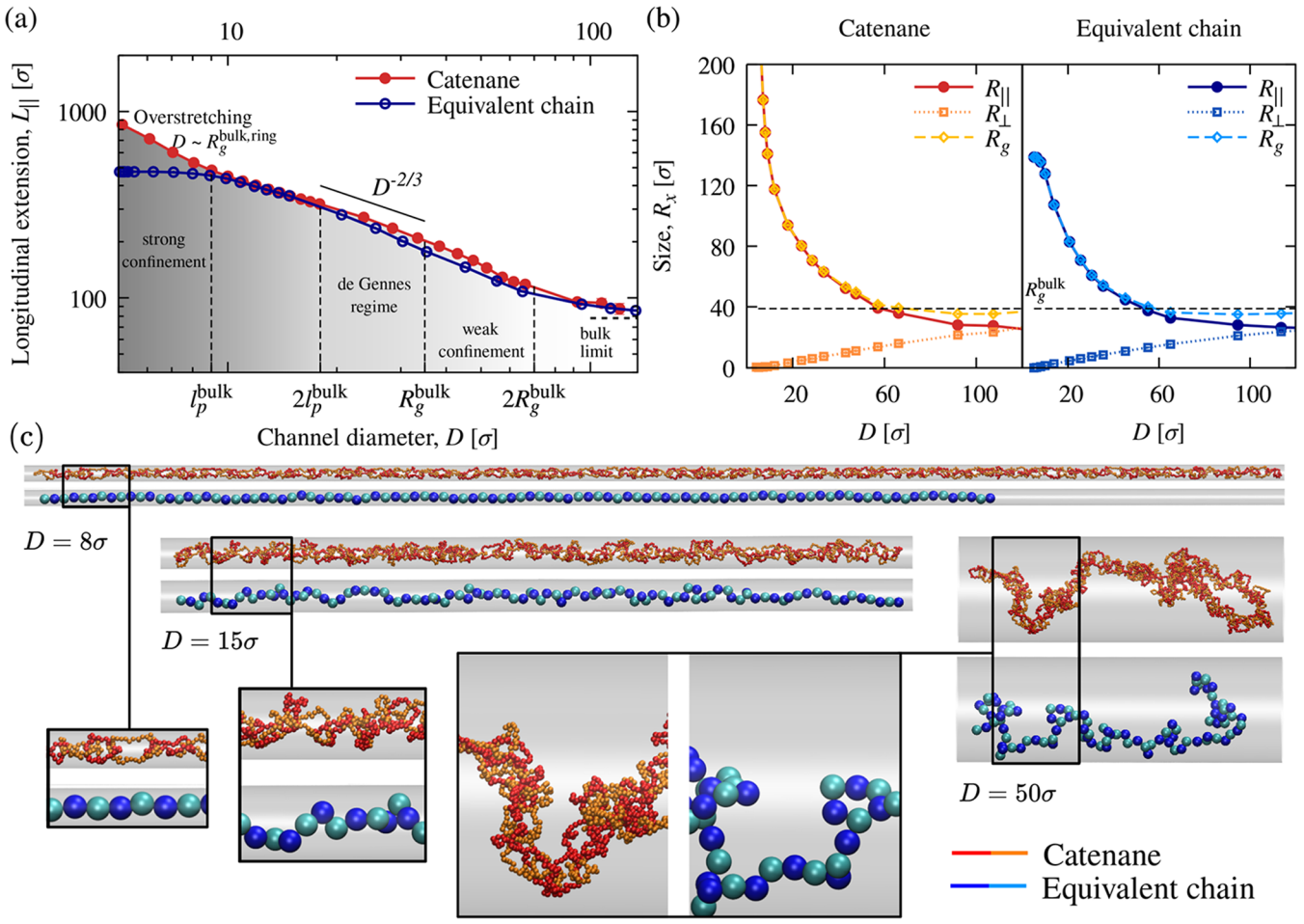

Figure 2. Scaling regimes of polycatenanes in channel confinement, and comparison with linear polymers. (a) The longitudinal extension of the catenane backbone, $L_{||}$, shows different confinement regimes as the channel diameter D decreases, as illustrated in the log−log plot. In the de Gennes regime, the best-fit estimates of the scaling exponent are -0.73 ± 0.03 for catenanes and -0.85 ± 0.01 for the equivalent chain. Panel b illustrates the variations of the catenanes' gyration radius, and of the longitudinal and transverse components, as a function of D. Analogous observables but measured for equivalent linear chains are also shown in (a) and (b). Error bars (shown) are typically smaller than data point symbols. Typical configurations of the catenane and equivalent chains at three different confinements are shown in (c), along with magnified views of their local features.

concatenated rings. Finally, Figure 4c displays the b/R_g^{ring} ratio as a function of D, which clarifies that b grows significantly already in the de Gennes regime, when R_g^{ring} is still relatively unaffected by confinement. It is interesting that the b/R_g^{ring} ratio varies even in strong confinement, where one could instead expect an increased coupling of the average extensions of rings and mechanical bonds. At the same time, the *fluctuations* around the average of ring size and mechanical bond length are increasingly correlated with growing confinement; see Figure S6.

By combining the results from Figures 2−4, we can gain a deeper understanding of how channel confinement affects catenanes. Moving from weak confinement to the de Gennes regime leaves isolated rings relatively unaffected, while mechanically bonded rings are drawn slightly closer, as evidenced by the decrease in b, and the catenane's backbone extends longitudinally. As strong confinement is approached, concatenated rings arrange approximately in single file, increasing their longitudinal extension and, especially, their separation. The increase of the mechanical bond length becomes even more pronounced in strong confinement, in both absolute terms and relative to the rings' extension. This increase is arguably fostered by the entropic segregation forces acting on confined rings,[28,36] which favors the tightening of interlocked regions.

Ring Deformation and Alignment. We next addressed the separate contributions that channel confinement and mechanical bonding make to the extension of the concatenated rings. To this end, we compared the gyration tensors of concatenated and isolated rings at different confinements.

We first considered the ranked square-rooted eigenvalues of the gyration tensor, $\lambda_{1,2,3}$; see Model and Methods. The average λ's as a function of D are presented in Figure 5a. The curves remain approximately constant down to $D \sim 15\sigma$. This indicates that concatenated rings maintain approximately the same size and shape as in unconstrained catenanes down to the end of the de Gennes regime, $D \sim 2l_p^{bulk} \sim 18\sigma$. Stronger confinements cause the simultaneous increase of λ_1 and a widening of its gaps with λ_2 and λ_3, due to the ring's extension and anisotropy growing in parallel.

The dashed curves in Figure 5a are for isolated rings. Compared to the concatenated case, $\lambda_{1,2}$ of isolated rings are systematically lower by 25% or more down to $D \sim 15\sigma$. This difference gradually reduces, in both relative and absolute

https://doi.org/10.1021/acs.macromol.3c00249
Macromolecules 2023, 56, 2736−2746

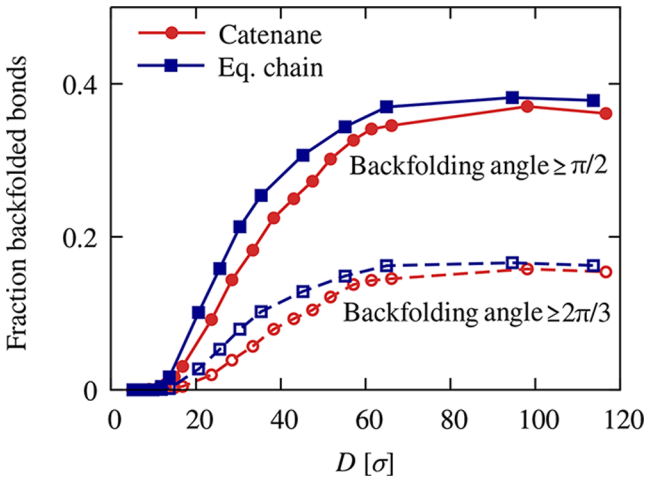

Figure 3. Backfolding of confined catenanes. Fraction of backfolded mechanical bonds in catenanes as a function of the channel diameter. A bond was considered as backfolded if the angle formed with the catenane's end-to-end vector was larger than a threshold value, θ. The curves are for two threshold angles, $\theta = \{\pi/2, 2\pi/3\}$. Analogous data but computed for equivalent chains are shown, too. Error bars are smaller than data point symbols.

terms, in the strong confinement regime. λ_3 remains mostly similar for catenated and isolated rings.

From the comparison, we conclude that, in the de Gennes and weak confinement regimes, mechanically bonded rings mostly retain the same shape as the unconstrained case, where mutual topological constraints make them larger and more planar than isolated (unconcatenated) rings. Although the size and shape of concatenated and isolated rings are approximately unchanged down to $D \sim 13\sigma$, their spatial orientations vary significantly, and in entirely different ways. This result is illustrated in Figure 5b, which presents the longitudinal components of the principal axes of the gyration ellipsoid, $e^{\parallel}_{1,2,3}$, with the values 0 and 1 corresponding to directions exactly orthogonal and parallel to the channel axis, respectively.

The three $e^{\parallel}$ curves for isolated rings remain superposed down to the end of the de Gennes regime, $D \sim 18\sigma$. Their common value of 0.5 is indicative of a lack of orientation bias. In fact, at these levels of confinement, the distribution of ring orientations is isotropic; see Figure S4. Only for $D < 13\sigma$, a gap opens between the $e^{\parallel}_1$ and $e^{\parallel}_3$ and progressively widens as the two quantities approach 1 and 0, respectively, in strong confinement.

Rings that are part of catenanes have starkly different behavior, exhibiting a gap between $e^{\parallel}_1$ and $e^{\parallel}_3$ even at $D = 30\sigma$, i.e., at channel widths that are too large to affect rings' size and shape. The gap grows rapidly with D. At $D = 13\sigma$, below the de Gennes regime, $e^{\parallel}_1 \sim 0.6$ is about twice $e^{\parallel}_3 \sim 0.3$. Note that, at the same width, isolated rings are still randomly oriented.

The data reveal a further qualitative difference. For isolated rings, it is only the principal gyration axis, $\hat{e}_1$ that aligns to the channel axis, while $\hat{e}_2$ and $\hat{e}_3$ become increasingly orthogonal to it. Instead, for concatenated rings, the increasing alignment of $\hat{e}_1$ toward the channel axis is accompanied by that of $\hat{e}_2$ throughout the de Gennes regime. Only for $D \lesssim 13\sigma$, $\hat{e}_2$ reverses its orientation, eventually becoming orthogonal to the channel axis, and more so than isolated rings. Additionally, $e^{\parallel}_3$ of concatenated rings is systematically smaller than that for isolated rings, particularly in the de Gennes regime.

To investigate the coupling between the orientation of the rings and mechanical bonds, we considered the scalar product between $\hat{e}_{1,2,3}$ of the central ring and $\hat{b}$, the normalized mechanical bond vector with one of the two linked neighbors. Figure 5c shows that, for $D \sim 13\sigma$, the average scalar products are about constant and equal to 0.6 for $\hat{b}\cdot\hat{e}_1$ and $\hat{b}\cdot\hat{e}_2$, while $\hat{b}\cdot\hat{e}_3$ is about half this value. This indicates that mechanical bonds in weak and de Gennes confinements tend to lie in the osculating plane of the rings, which are approximately planar. However, for $D < 13\sigma$, i.e., approaching and entering strong confinement, $\hat{b}$ becomes increasingly parallel to $\hat{e}_1$ and orthogonal to $\hat{e}_{2,3}$.

Several conclusions can be drawn for the combined effects of mechanical bonding and confinement on the rings. First, even at weak confinement, the orientation of the concatenated rings, which are quasi-planar, is biased, the normals of their osculating planes tending to be orthogonal to the channel axis. This bias is a genuine product of the concatenation constraint or mechanical bonding. Second, the orientational bias grows until the end of the de Gennes regime. Finally, in

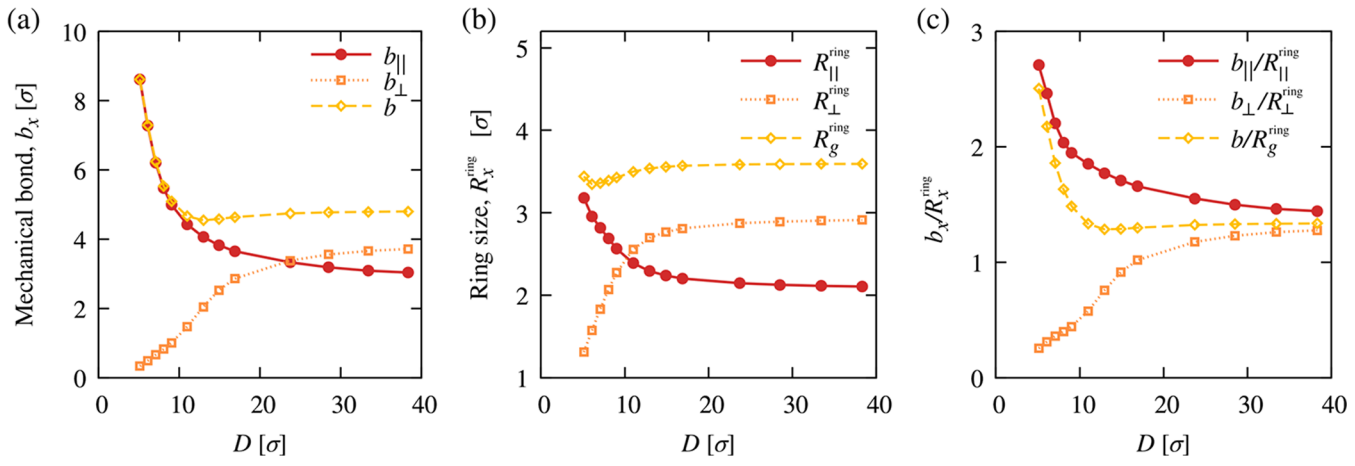

Figure 4. Response of mechanical bonds and ring size to confinement. The variations as a function of the channel diameter, D, of the average length of mechanical bonds and the rings' gyration radii are shown in (a) and (b), respectively. The longitudinal and transverse components of the two observables are shown, too. The adimensional ratio of the mechanical bond and ring size, and their longitudinal and transverse components, are shown in (c). Error bars are smaller than data point symbols.

https://doi.org/10.1021/acs.macromol.3c00249
Macromolecules 2023, 56, 2736−2746

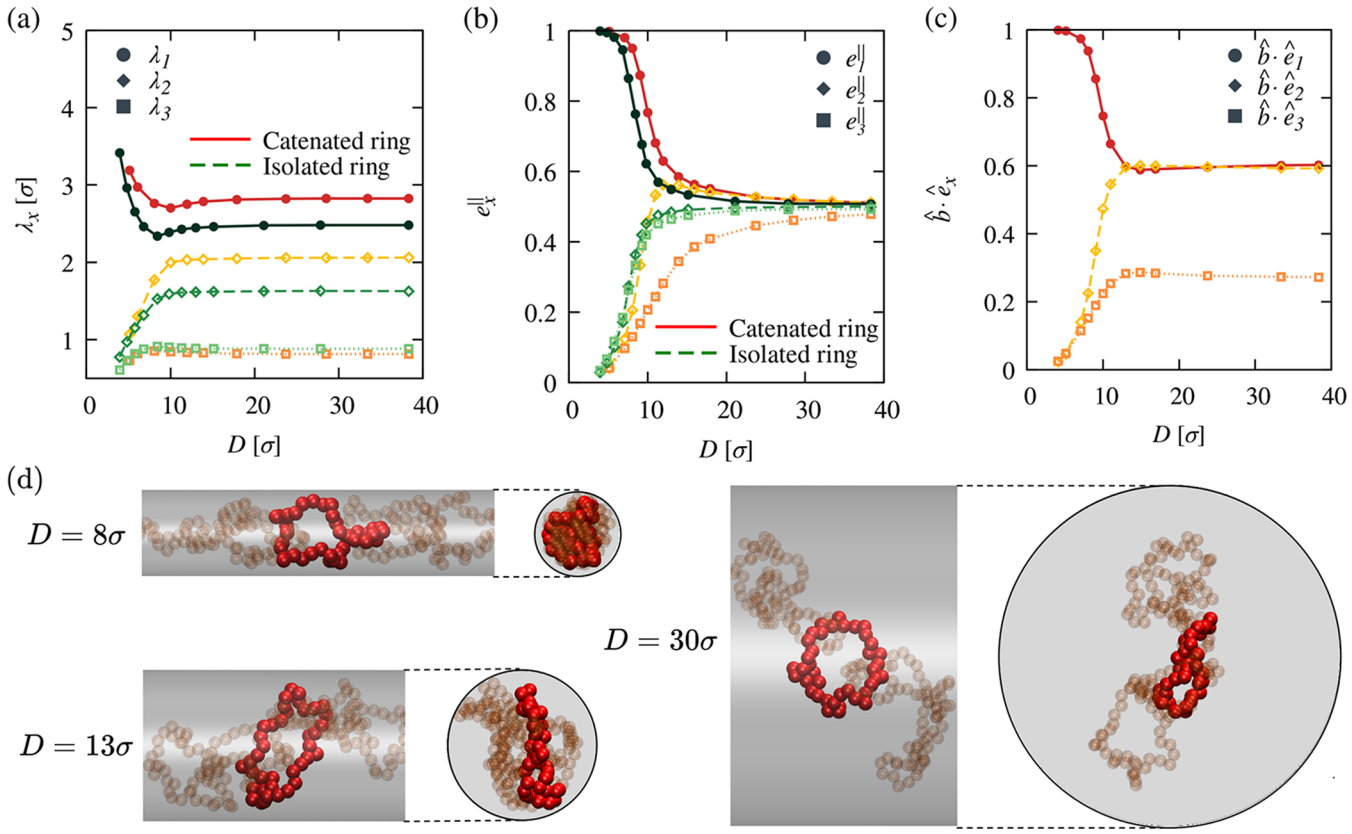

Figure 5. Ring shape and orientation in confinement. (a) The ranked root-squared eigenvalues of the gyration tensor of concatenated rings, $\lambda_{1,2,3}$, are shown as a function of the channel diameter, D. For comparison, the same quantities, but computed for an isolated (unconcatenated) ring are shown, too. Panel b illustrates the D dependence of the longitudinal components of the normalized eigenvectors of the gyration tensor of concatenated and isolated rings, $\hat{e}_{1,2,3}$. The relative orientation of a concatenated ring and one of its two mechanical bonds is shown in (c) through the scalar products of the normalized mechanical bond, $\hat{b}$, and $\hat{e}_{1,2,3}$. The changes in shape and orientation of concatenated rings are illustrated by the typical configurations in (d), presenting longitudinal and transverse views of short sections of the catenanes at different confinements. Error bars are smaller than data point symbols.

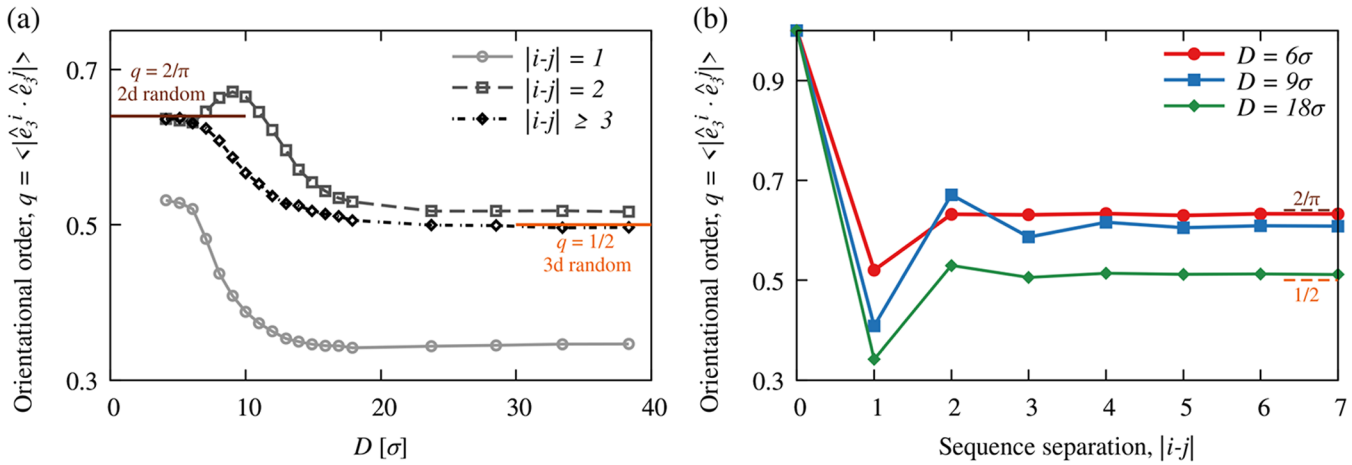

Figure 6. Orientational order of rings along the backbone. (a) Average absolute scalar product between rings' osculating plane directions, $\hat{e}_3^i$ and $\hat{e}_3^j$, versus channel diameter D for different values of sequence separations $|i - j|$. For randomly oriented vectors there are two different limits going from three dimensions ($D \to \infty$) to two dimensions ($D \to 0$, where $\hat{e}_3$ is effectively constrained on the plane orthogonal to the channel axis). (b) Same quantity plotted versus sequence separation, for three values of D. Error bars are smaller than data point symbols.

strong confinement, $D \lesssim 13\sigma$, concatenated rings deform, changing size and shape, becoming uniaxially anisotropic. These concurrent geometrical variations are evident in the configurations of Figure 5d.

Orientational Correlation of Concatenated Rings. We next examined the orientational correlation of rings at various distances along the catenane backbone. To measure the correlation, we considered all pairs of concatenated rings, i and j, and computed the average scalar products of the normals to

https://doi.org/10.1021/acs.macromol.3c00249
Macromolecules 2023, 56, 2736−2746

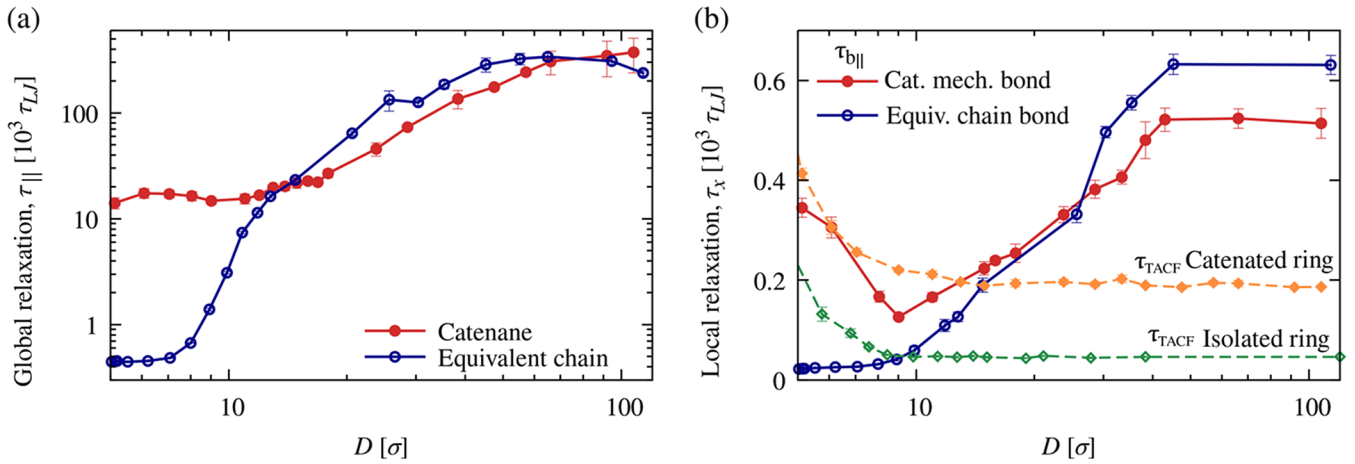

Figure 7. Global and local relaxation times. (a) Autocorrelation time of the longitudinal extension $L_{\|}$ plotted against channel diameter D for catenane (red) and equivalent chain (blue). (b) Autocorrelation times for local observables: longitudinal component of a mechanical bond in catenanes (red); longitudinal component of a covalent bond in the equivalent chain (blue); rotational time of ring diameters for catenated rings (dashed orange) and isolated rings (dashed green).

the osculating planes, $q \equiv \langle |\hat{e}_3^i \cdot \hat{e}_3^j| \rangle$ for increasing sequence separations, $|i - j|$. As a reference, we note that, for randomly oriented vectors in three and two dimensions, one has $q = 1/2$ and $q = 2/\pi$, respectively.

The average values of q as a function of sequence separation and channel width are shown in Figure 6. The probability distributions of q for selected values of $|i - j|$ and D are shown in Figure S5. The data reveal that consecutive rings, $|i - j| = 1$, have a much lower value of q than rings at larger sequence separations. The propagation of this orthogonality bias reflects in the coplanarity tendency of next-nearest-neighboring rings, which have the largest q values. These properties are in line with those previously found for unconstrained catenanes[24] and thus clarify that the concatenation-induced bias of consecutive rings toward being orthogonal is maintained through moderate confinement.

The orientational correlation of next-nearest-neighboring rings, equivalent to a nematic ordering of their normals, becomes stronger through the weak and de Gennes confinement regimes and is maximum at $D \sim 9\sigma$. The data in Figure 6b indicate that the correlation is short-ranged at all values of D, extending over only a few mechanical bonds before settling to the value for randomly oriented unit vectors. We recall that the latter is equal to $1/2$ in three dimensions, which is pertinent to large channels, and is equal to $2/\pi$ in two dimensions, which is pertinent for uniaxially anisotropic ringsModel and Methods.

We also note that a similarly short correlation range was previously reported for the influence of mechanical bonding on the statics and dynamics of free catenanes.[15,24,25]

The data of Figure 6 thus show that the nematic ordering of rings with even and odd indices persists in channels and is largest at the onset of strong confinement ($D \sim 9\sigma$). At these channel widths, concatenated rings themselves start to elongate, their shape changing from quasi-planar to uniaxially anisotropic, and the principal direction of the gyration tensor is increasingly aligned to the channel axis (Supporting Information). In response, major changes occur in the probability distributions for q, which switch from broad to sharply peaked, causing the observed nonmonotonicity for $|i - j| = 2$, as detailed in Figure S5.

Dynamic Properties. Building on studies of channel-confined polymers,[30−33,47,48] we studied the global relaxation dynamics of unconstrained catenanes through the autocorrelation time of the longitudinal extension, $\tau_{\|}$.

The D dependence of the catenane's $\tau_{\|}$ is presented in Figure 7a. The figure also shows $\tau_{\|}$ for the equivalent chain, which is defined by a mapping that, among various quantities, matches the diffusion coefficient of the systems in the absence of confinement; see Model and Methods and Table S1. At the largest channels, $D > 60\sigma$, the extensional relaxation times of catenanes and equivalent chains are compatible within statistical errors. The $\tau_{\|}$ curve of the equivalent chain, better defined thanks to the smaller statistical uncertainty, features a maximum for $D \sim 65\sigma$; see also Figure S8 for a linear version of the plot. The nonmonotonicity of $\tau_{\|}$ is similar to that observed for channel-confined DNA.[49] However, the maximum $\tau_{\|}$ for DNA is located at the crossover of the Odijk and extended de Gennes regimes,[31,32] while in our system, where persistence length and thickness are comparable, is found in weak confinement.

For $D < 70\sigma$, the $\tau_{\|}$ curves of the catenane and equivalent chain decrease significantly down to $D \sim 13\sigma$, dropping by more than an order of magnitude respect to the wide channels limit ($D \sim 100\sigma$). Increasing confinement further elicits a very different relaxation response of the two systems, with the catenane's $\tau_{\|}$ remaining about constant at $1.5 \times 10^4 \tau_{LJ}$. In comparison, that of the equivalent chain decreases by 1 order of magnitude as D approaches 5σ.

The comparison establishes the following results. First, increasing channel confinement makes the catenanes' global relaxation dynamics systematically faster. Down to the onset of the strong confinement regime, the relaxation times decrease in an aspecific manner, meaning that a similar decrease occurs for equivalent polymer chains with covalently bonded monomers. The specificity of mechanical bonding emerges in strong confinement, with catenane's $\tau_{\|}$ remaining approximately constant, while that of the equivalent polymer further decreases significantly.

Finally, we studied the catenane's relaxation modes at the local scale, i.e., for isolated rings and mechanical bonds. For the internal dynamics of the rings, we used τ_{TACF}, the decay time of the so-called terminal autocorrelation function, which is the

https://doi.org/10.1021/acs.macromol.3c00249
Macromolecules 2023, 56, 2736−2746

time-lagged orientation correlation function of the rings' diameters.[45] In addition, we computed the characteristic correlation time of the longitudinal projection of mechanical bonds, $\tau_{b_\parallel}$.

As revealed by Figure 7b, in wide channels, the relaxation of mechanical bonds is slower than the rings' internal one by a factor of 3. Notice that the catenanes' $\tau_{b_\parallel}$ is close to the equivalent chain's one. The results reveal that, in wide channels, the relaxation dynamics of mechanical bonds is more strongly coupled to the (slow) modes of the catenane's backbone than the internal dynamics of the rings. The decoupling of the two local relaxation mechanisms persists throughout the entire de Gennes regime. In fact, $\tau_{b_\parallel}$ decreases systematically to $D = 9\sigma$, even falling below τ_{TACF}, while the latter remains approximately constant.

However, as the catenane becomes strongly confined, $D < 9\sigma$, both τ_{TACF} and $\tau_{b_\parallel}$ increase. The common increasing trend, and the fact that the two time scales remain comparable down to $D = 5\sigma$, indicates that the modes are now coupled. Thus, in the approximately single-file ring arrangement caused by strong confinement, the fluctuations of the mechanical bond extensions largely follow the conformational changes of the rings, which modulate the intermingling of the rings. This conclusion is supported by the comparison with the equivalent chain, where the coupling of $\tau_{b_\parallel}$ and τ_{TACF} is absent.

DISCUSSION AND CONCLUSION

We studied the effect of confinement on the statics and dynamics of catenanes, comparing results to equivalent chains to single out specific effects of mechanical bonding.

The catenane's confinement extension presents different regimes, depending on how the channel width compares to intrinsic length scales, such as the gyration radius and persistence length of the unconstrained catenane, R_g and l_p, and of the rings, R_g^{ring}. A weak elongation response is first observed at $D \sim 2R_g$, followed by a de Gennes regime D between R_g and $2l_p$. At $D \sim l_p$, R_g^{ring}, there is a crossover to the strong confinement regime, where the catenane's and equivalent polymer's behaviors diverge. The polymer extension saturates and levels off, while that of the catenanes continues to grow. This overstretching regime is underpinned by the internal degrees of freedom associated with mechanical bonding, allowing for distance fluctuations of concatenated rings even when strongly elongated.

Examining local properties, we observed a significant longitudinal alignment of mechanical bonds even in weak confinement. In contrast, both the shape and size of isolated rings remain almost unchanged through the de Gennes regime. In the strong confinement regime, the size and shape of the rings are also strongly impacted, acquiring the expected uniaxial anisotropy. Comparison with isolated (nonconcatenated) rings subjected to the same degree of confinement clarifies that the mechanical bonding constraint makes the uniaxial anisotropy stronger under strong confinement. Surprisingly, however, mechanical bonding causes a much greater planarity of the rings in the regimes of weak confinement and de Gennes confinement.

Finally, we examined the relaxation dynamics, observing that confinement typically makes it faster. Specifically, the longitudinal extension relaxation times decrease by more than an order of magnitude through weak and de Gennes confinement regimes. This decrease is largely aspecific, as it is observed in equivalent polymers, too. However, major differences are observed in confinement, with the catenane's relaxation time remaining approximately constant while the polymer's one drops by more than an order of magnitude. The analysis of the microscopic dynamics, i.e., the relaxation of mechanical bonds, clarifies that this slow dynamics unique to catenanes originates from a specific slow mode, namely the longitudinal sliding of strongly elongated concatenated rings.

The above results provide a first insight into the response of catenanes to channel confinement, a setup that is commonly used for linear polymers. Besides providing a reference to inspire and inform the design of possible confinement experiments, the findings suggest several extensions, from applicative to more general ones. The former include the entropic sorting of catenanes using elongational flows in corrugated channels[50−55] or harnessing topological friction in nanopore translocation setups.[56−58] It would also be important to investigate scaling properties, such as the effects of catenane length, ring size, and the dimensionality of the confining regions, as well as hydrodynamic effects. For the latter, it would interesting to ascertain whether the decoupling of hydrodynamic and topological interactions previously observed in unconstrained linked ring polymers[59] holds in spatial confinement too.

ASSOCIATED CONTENT

Supporting Information

The Supporting Information is available free of charge at https://pubs.acs.org/doi/10.1021/acs.macromol.3c00249.

Additional details for the statics and dynamics of confined catenanes and equivalent chains (PDF)

AUTHOR INFORMATION

Corresponding Author

Cristian Micheletti − *International School for Advanced Studies (SISSA), 34136 Trieste, Italy;* orcid.org/0000-0002-1022-1638; Email: cristian.micheletti@sissa.it

Author

Pietro Chiarantoni − *International School for Advanced Studies (SISSA), 34136 Trieste, Italy;* orcid.org/0000-0002-9249-863X

Complete contact information is available at: https://pubs.acs.org/10.1021/acs.macromol.3c00249

Notes

The authors declare no competing financial interest.

REFERENCES

(1) Wu, Q.; Rauscher, P. M.; Lang, X.; Wojtecki, R. J.; de Pablo, J. J.; Hore, M. J. A.; Rowan, S. J. Poly[n]catenanes: Synthesis of molecular interlocked chains. *Science* **2017**, *358*, 1434−1439.

(2) Datta, S.; Kato, Y.; Higashiharaguchi, S.; Aratsu, K.; Isobe, A.; Saito, T.; Prabhu, D. D.; Kitamoto, Y.; Hollamby, M. J.; Smith, A. J.; et al. Self-assembled poly-catenanes from supramolecular toroidal building blocks. *Nature* **2020**, *583*, 400−405.

(3) Collier, C. P.; Mattersteig, G.; Wong, E. W.; Luo, Y.; Beverly, K.; Sampaio, J.; Raymo, F. M.; Stoddart, J. F.; Heath, J. R. A [2]Catenane-Based Solid State Electronically Reconfigurable Switch. *Science* **2000**, *289*, 1172−1175.

(4) Kay, E. R.; Leigh, D. A. Beyond switches: Rotaxane-and catenane-based synthetic molecular motors. *Pure Appl. Chem.* **2008**, *80*, 17−29.
(5) Niu, Z.; Gibson, H. W. Polycatenanes. *Chem. Rev.* **2009**, *109*, 6024−6046.
(6) Gil-Ramírez, G.; Leigh, D. A.; Stephens, A. J. Catenanes: Fifty Years of Molecular Links. *Angew. Chem., Int. Ed.* **2015**, *54*, 6110−6150.
(7) Meng, Z.; Han, Y.; Wang, L.-N.; Xiang, J.-F.; He, S.-G.; Chen, C.-F. Stepwise Motion in a Multivalent [2](3)Catenane. *J. Am. Chem. Soc.* **2015**, *137*, 9739−9745.
(8) August, D. P.; Borsley, S.; Cockroft, S. L.; Della Sala, F.; Leigh, D. A.; Webb, S. J. Transmembrane ion channels formed by a Star of David [2] catenane and a molecular pentafoil knot. *J. Am. Chem. Soc.* **2020**, *142*, 18859−18865.
(9) Hart, L. F.; Hertzog, J. E.; Rauscher, P. M.; Rawe, B. W.; Tranquilli, M. M.; Rowan, S. J. Material properties and applications of mechanically interlocked polymers. *Nature Reviews Materials* **2021**, *6*, 508−530.
(10) Orlandini, E.; Micheletti, C. Topological and physical links in soft matter systems. *J. Phys.: Condens. Matter* **2022**, *34*, 013002.
(11) Liu, G.; Rauscher, P. M.; Rawe, B. W.; Tranquilli, M. M.; Rowan, S. J. Polycatenanes: synthesis, characterization, and physical understanding. *Chem. Soc. Rev.* **2022**, *51*, 4928−4948.
(12) Polles, G.; Orlandini, E.; Micheletti, C. Optimal Self-Assembly of Linked Constructs and Catenanes via Spatial Confinement. *ACS Macro Lett.* **2016**, *5*, 931−935.
(13) Caraglio, M.; Orlandini, E.; Whittington, S. G. Driven Translocation of Linked Ring Polymers through a Pore. *Macromol.* **2017**, *50*, 9437−9444.
(14) Caraglio, M.; Micheletti, C.; Orlandini, E. Mechanical Pulling of Linked Ring Polymers: Elastic Response and Link Localisation. *Polymers* **2017**, *9*, 327.
(15) Rauscher, P. M.; Rowan, S. J.; de Pablo, J. J. Topological Effects in Isolated Poly[n]catenanes: Molecular Dynamics Simulations and Rouse Mode Analysis. *ACS Macro Lett.* **2018**, *7*, 938−943.
(16) Ahmadian Dehaghani, Z.; Chubak, I.; Likos, C. N.; Ejtehadi, M. R. Effects of topological constraints on linked ring polymers in solvents of varying quality. *Soft Matter* **2020**, *16*, 3029−3038.
(17) Soh, B. W.; Doyle, P. S. Deformation Response of Catenated DNA Networks in a Planar Elongational Field. *ACS Macro Lett.* **2020**, *9*, 944−949.
(18) Klotz, A. R.; Soh, B. W.; Doyle, P. S. Equilibrium structure and deformation response of 2D kinetoplast sheets. *Proc. Natl. Acad. Sci. U.S.A.* **2020**, *117*, 121−127.
(19) Meng, W.; Kondo, S.; Ito, T.; Komatsu, K.; Pirillo, J.; Hijikata, Y.; Ikuhara, Y.; Aida, T.; Sato, H. An elastic metal−organic crystal with a densely catenated backbone. *Nature* **2021**, *598*, 298−303.
(20) Soh, B. W.; Doyle, P. S. Equilibrium Conformation of Catenated DNA Networks in Slitlike Confinement. *ACS Macro Lett.* **2021**, *10*, 880−885.
(21) Tubiana, L.; Ferrari, F.; Orlandini, E. Circular Polycatenanes: Supramolecular Structures with Topologically Tunable Properties. *Phys. Rev. Lett.* **2022**, *129*, 227801.
(22) Li, J.; Gu, F.; Yao, N.; Wang, H.; Liao, Q. Double Asymptotic Structures of Topologically Interlocked Molecules. *ACS Macro Lett.* **2021**, *10*, 1094−1098.
(23) Rauscher, P. M.; Schweizer, K. S.; Rowan, S. J.; de Pablo, J. J. Dynamics of poly[n]catenane melts. *J. Chem. Phys.* **2020**, *152*, 214901.
(24) Chiarantoni, P.; Micheletti, C. Effect of Ring Rigidity on the Statics and Dynamics of Linear Catenanes. *Macromolecules* **2022**, *55*, 4523−4532.
(25) Rauscher, P. M.; Schweizer, K. S.; Rowan, S. J.; de Pablo, J. J. Thermodynamics and Structure of Poly[n]catenane Melts. *Macromolecules* **2020**, *53*, 3390−3408.
(26) Lei, H.; Zhang, J.; Wang, L.; Zhang, G. Dimensional and shape properties of a single linear polycatenane: Effect of catenation topology. *Polymer* **2021**, *212*, 123160.
(27) Chen, Y.-X.; Cai, X.-Q.; Zhang, G.-J. Topological Catenation Enhances Elastic Modulus of Single Linear Polycatenane. *Chin. J. Polym. Sci.* **2023**, DOI: 10.1007/s10118-023-2902-x.
(28) Amici, G.; Caraglio, M.; Orlandini, E.; Micheletti, C. Topologically linked chains in confinement. *ACS Macro Lett.* **2019**, *8*, 442−446.
(29) Amici, G.; Caraglio, M.; Orlandini, E.; Micheletti, C. Topological Friction and Relaxation Dynamics of Spatially Confined Catenated Polymers. *ACS Macro Lett.* **2022**, *11*, 1−6.
(30) Milchev, A. Single-polymer dynamics under constraints: scaling theory and computer experiment. *J. Phys.: Condens. Matter* **2011**, *23*, 103101.
(31) Reisner, W.; Pedersen, J. N.; Austin, R. H. DNA confinement in nanochannels: physics and biological applications. *Rep. Prog. Phys.* **2012**, *75*, 106601.
(32) Wang, Y.; Tree, D. R.; Dorfman, K. D. Simulation of DNA Extension in Nanochannels. *Macromolecules* **2011**, *44*, 6594−6604.
(33) Cifra, P.; Benková, Z.; Bleha, T. Chain extension of DNA confined in channels. *J. Phys. Chem. B* **2009**, *113*, 1843−1851.
(34) Cheong, G. K.; Li, X.; Dorfman, K. D. Evidence for the extended de Gennes regime of a semiflexible polymer in slit confinement. *Phys. Rev. E* **2018**, *97*, 022502.
(35) Ma, Z.; Dorfman, K. D. Diffusion of Knots along DNA Confined in Nanochannels. *Macromolecules* **2020**, *53*, 6461−6468.
(36) Arnold, A.; Jun, S. Time scale of entropic segregation of flexible polymers in confinement: Implications for chromosome segregation in filamentous bacteria. *Phys. Rev. E* **2007**, *76*, 031901.
(37) Hoseinpoor, S. M.; Nikoofard, N.; Zahedifar, M. Accuracy Limits of the Blob Model for a Flexible Polymer Confined Inside a Cylindrical Nano-Channel. *J. Stat. Phys.* **2016**, *163*, 593−603.
(38) Jung, Y.; Jun, S.; Ha, B.-Y. Self-avoiding polymer trapped inside a cylindrical pore: Flory free energy and unexpected dynamics. *Phys. Rev. E* **2009**, *79*, 061912.
(39) Reisner, W.; Morton, K. J.; Riehn, R.; Wang, Y. M.; Yu, Z.; Rosen, M.; Sturm, J. C.; Chou, S. Y.; Frey, E.; Austin, R. H. Statics and dynamics of single DNA molecules confined in nanochannels. *Physical review letters* **2005**, *94*, 196101.
(40) Chen, Y.-L.; Lin, Y.-H.; Chang, J.-F.; Lin, P.-k. Dynamics and Conformation of Semiflexible Polymers in Strong Quasi-1D and −2D Confinement. *Macromolecules* **2014**, *47*, 1199−1205.
(41) Kremer, K.; Grest, G. S. Dynamics of entangled linear polymer melts: A molecular-dynamics simulation. *J. Chem. Phys.* **1990**, *92*, 5057−5086.
(42) Plimpton, S. Fast parallel algorithms for short-range molecular dynamics. *J. Comput. Phys.* **1995**, *117*, 1−19.
(43) Muralidhar, A.; Tree, D. R.; Dorfman, K. D. Backfolding of Wormlike Chains Confined in Nanochannels. *Macromolecules* **2014**, *47*, 8446−8458.
(44) Müller, M.; Wittmer, J.; Cates, M. Topological effects in ring polymers: A computer simulation study. *Phys. Rev. E* **1996**, *53*, 5063.
(45) Katsarou, A. F.; Tsamopoulos, A. J.; Tsalikis, D. G.; Mavrantzas, V. G. Dynamic heterogeneity in ring-linear polymer blends. *Polymers* **2020**, *12*, 752.
(46) Marko, J. F. DNA under high tension: Overstretching, undertwisting, and relaxation dynamics. *Phys. Rev. E* **1998**, *57*, 2134−2149.
(47) Bonthuis, D. J.; Meyer, C.; Stein, D.; Dekker, C. Conformation and dynamics of DNA confined in slitlike nanofluidic channels. *Physical review letters* **2008**, *101*, 108303.
(48) Odijk, T. Scaling theory of DNA confined in nanochannels and nanoslits. *Phys. Rev. E* **2008**, *77*, 060901.
(49) Reisner, W.; Morton, K. J.; Riehn, R.; Wang, Y. M.; Yu, Z.; Rosen, M.; Sturm, J. C.; Chou, S. Y.; Frey, E.; Austin, R. H. Statics and Dynamics of Single DNA Molecules Confined in Nanochannels. *Phys. Rev. Lett.* **2005**, *94*, 196101.
(50) Tessier, F.; Labrie, J.; Slater, G. W. Electrophoretic separation of long polyelectrolytes in submolecular-size constrictions: a Monte Carlo study. *Macromolecules* **2002**, *35*, 4791−4800.

(51) D'Agostino, T.; Salis, S.; Ceccarelli, M. A kinetic model for molecular diffusion through pores. *Biochimica et Biophysica Acta (BBA)-Biomembranes* **2016**, *1858*, 1772−1777.
(52) Marenda, M.; Orlandini, E.; Micheletti, C. Sorting ring polymers by knot type with modulated nanochannels. *Soft Matter* **2017**, *13*, 795−802.
(53) Kim, D.; Bowman, C.; Del Bonis-O'Donnell, J. T.; Matzavinos, A.; Stein, D. Giant acceleration of DNA diffusion in an array of entropic barriers. *Phys. Rev. Lett.* **2017**, *118*, 048002.
(54) Weiss, L. B.; Marenda, M.; Micheletti, C.; Likos, C. N. Hydrodynamics and filtering of knotted ring polymers in nanochannels. *Macromolecules* **2019**, *52*, 4111−4119.
(55) Bodrenko, I. V.; Salis, S.; Acosta-Gutierrez, S.; Ceccarelli, M. Diffusion of large particles through small pores: From entropic to enthalpic transport. *J. Chem. Phys.* **2019**, *150*, 211102.
(56) Suma, A.; Rosa, A.; Micheletti, C. Pore Translocation of Knotted Polymer Chains: How Friction Depends on Knot Complexity. *ACS Macro Lett.* **2015**, *4*, 1420−1424.
(57) Caraglio, M.; Orlandini, E.; Whittington, S. G. Translocation of links through a pore: effects of link complexity and size. *J. Stat. Mech.: Theory and Exp.* **2020**, *2020*, 043203.
(58) Rheaume, S. N.; Klotz, A. R. Nanopore translocation of topologically linked DNA catenanes. *Phys. Rev. E* **2023**, *107*, 024504.
(59) Rauscher, P. M.; Rowan, S. J.; de Pablo, J. J. Hydrodynamic interactions in topologically linked ring polymers. *Phys. Rev. E* **2020**, *102*, 032502.

https://doi.org/10.1021/acs.macromol.3c00249
Macromolecules 2023, 56, 2736−2746